



**Journal of
Mechanics of
Materials and Structures**

**ANALYTICAL ESTIMATES FOR THE LATERAL THRUST IN BOLTED STEEL
BUCKLING-RESTRAINED BRACES**

Guido Bregoli, Francesco Genna and Giovanni Metelli

Volume 11, No. 2

March 2016



ANALYTICAL ESTIMATES FOR THE LATERAL THRUST IN BOLTED STEEL BUCKLING-RESTRAINED BRACES

GUIDO BREGOLI, FRANCESCO GENNA AND GIOVANNI METELLI

Analytical expressions are developed for the lateral thrust exerted by the core of a buckling-restrained brace (BRB), when, upon a prescribed axial loading history, it buckles, coming into contact with the external retaining structure. Account is taken of (i) the elastic stiffness of the containment case; (ii) the possible flattened shape of each buckled wave in the zones of contact with the containment profiles; and (iii) the increase in the lateral thrust due to loading-unloading in the presence of linear kinematic hardening. Comparisons with both experimental and numerical results confirm the effectiveness of the analytical predictions. The proposed calculation techniques for the lateral thrust might be of help in the design procedures of BRBs.

1. Introduction

The design of buckling-restrained braces (BRB) is becoming an increasingly important topic in civil engineering, both because BRBs have been recognized to be effective in dissipating energy, and because they appear to be quite useful for structural upgrade with minimal interventions. Nevertheless, the behavior of BRBs is not yet understood in full. For example, reliable formulas are still lacking with reference to the design of the containing structure, an element expected to sustain large lateral forces deriving from the contact with the buckled internal core; these lateral forces, if not properly accounted for, can lead to the collapse, local or global, of the whole structural element.

Little attention seems to have been devoted, so far, to the calculation of the lateral thrust in BRBs as consequence of a given loading history. Basic engineering approaches can be found in [Lin et al. 2012; Takeuchi et al. 2010; Wu et al. 2014; Chou and Chen 2010; Zhao et al. 2014]; in these works a capacity design approach was often taken, with the aim of estimating only the maximum possible thrust acting on the retaining profiles, independently on the actual loading history. Moreover, a standard Euler's relation between applied axial load and buckled wavelength was always assumed, which is incorrect in the present situation.

Other work is mainly theoretical, such as that of [Chai 1998] which, however, considers the case of large displacements, which entails complications that are unneeded in BRB applications, where the gap between core and containment is usually very small. A brief discussion of the relevance of this type of work to the case of BRBs can be found in [Genna and Bregoli 2014].

The present paper illustrates new results that exploit the theory developed in [Genna and Bregoli 2014], where only a generic, fully elastic problem of buckling with frictionless contact was studied, for a monotonic loading condition only. The new results presented hereafter hold for BRBs in the elastic-plastic case, and account both for friction and, at least in part, for the effect of cyclic loading. The main

Keywords: buckling-restrained braces, elastic-plastic buckling, unilateral contact, lateral thrust, restraining member design.

goal is an attempt at obtaining working design expressions, for the lateral thrust in bolted steel BRBs, that could be considered reliable in engineering terms, despite the uncertainty of several governing parameters, such as the existing imperfections as well as the friction and the material properties.

The results thus obtained will be compared with available experimental and numerical ones described in detail elsewhere [Bregoli et al. 2014; Bregoli 2014; Genna and Gelfi 2012a].

2. Theoretical background

The structural element herein considered is illustrated in Figure 1, which refers to a BRB made of two main steel components: an internal plate, or core, which is the energy-dissipating element, and an external containment structure, that can be made of steel profiles, bolted to each other and designed so as to leave a nominal gap s between their internal surfaces and the external ones of the core.

The structural model of Figure 2 is adopted to describe the postbuckling mechanics of a steel-bolted BRB. In it, the central linear element represents the deformable core; the upper and lower linear elements represent the containment profiles, described as rigid surfaces free to translate only, and connected to

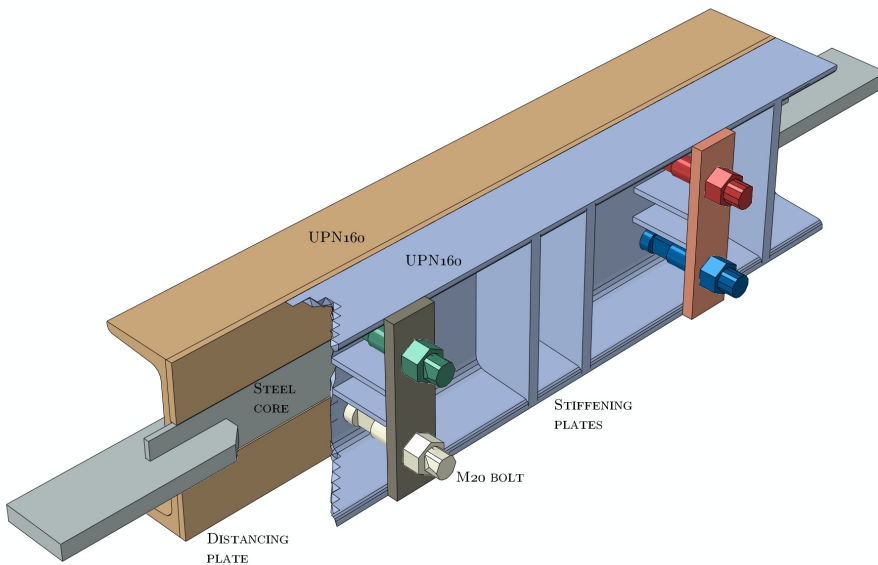


Figure 1. Sketch of the geometry of the studied BRB, showing the internal steel plate, the distancing plates, the two external C-shaped retaining steel profiles (one of them has been partially hidden), and the four connecting bolts. The transversal stiffening plates define an assembly called “design” in Section 6.

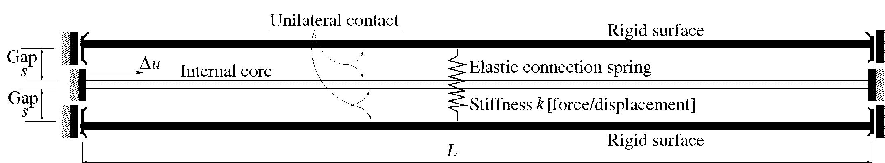


Figure 2. Analytical model for the study of a BRB assembly.

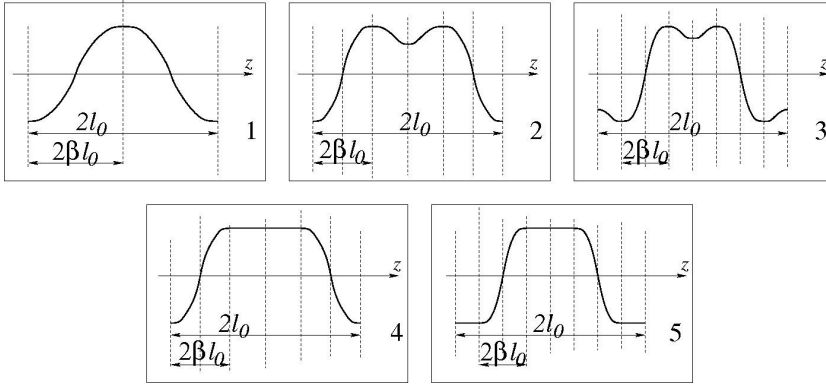


Figure 3. Buckled shapes (single waves shown): possible contact configurations considered in the analytical treatment. Image 1 is of a symmetric, single point contact. Image 2 is of an asymmetric point contact, which derives from the configuration of image 4 after local buckling of the flat top portion. Image 3 concerns a symmetric double point contact, deriving from the simultaneous local buckling of the flat portions in image 5. Image 4 is of an asymmetric line contact configuration, with line contact on top and point contact on bottom. Image 5 is of a symmetric line contact configuration.

each other by means of a linear elastic spring, with elastic constant k (dimension of force divided by displacement). This spring accounts for the actual deformability — both global and local — of the whole containment structure of [Figure 1](#). Assuming always small values of the gap s and small deflections, the analysis of this model is carried out in a second-order theory; shear strain contributions are neglected. It is assumed that the buckled configuration of the core is periodic, so that only half of a buckled wave needs to be studied. Throughout this paper, compression and shortening will be assumed as positive.

In order to consider the presence of line (flat) contacts between core and containment, it is assumed that the buckled shape can take any of the forms illustrated in [Figure 3](#), which are of 3 types: (i) a pure point contact configuration, which has 3 possible subcases: with a single contact point at each side of each wave (image 1); or with one contact point at one side and two contact points at the other side of the core (image 2); or with two contact points at each side of each wave (image 3); (ii) an asymmetric line contact configuration (image 4), and (iii) a symmetric line contact configuration (image 5).

In the sequel of this work, E denotes the Young modulus of the core, A the area of its cross-section, L its total length, F the compressive axial force existing in the buckled core, related to the axial shortening Δu , in the elastic range, by the expression

$$F = \frac{EA}{L} \Delta u. \quad (1)$$

Further, I denotes the minimum moment of inertia of the core, α the ratio defined by

$$\alpha^2 = \frac{F}{EI}, \quad (2)$$

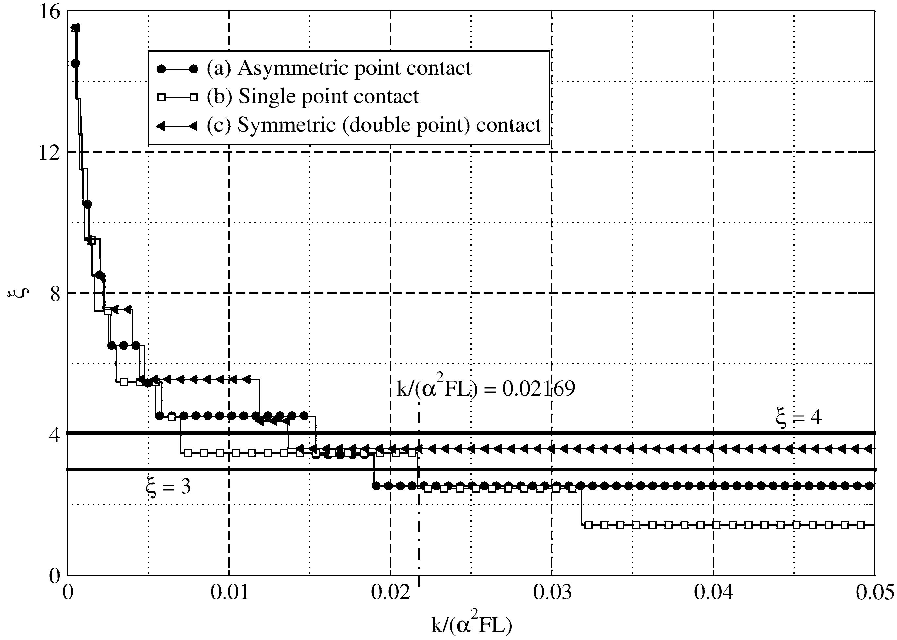


Figure 4. Possible values of ξ , defined in (4), as a function of the normalized spring stiffness $k/(\alpha^2 FL)$. The horizontal solid lines describe maximum values for ξ in the case of line contacts. The lines with symbols describe the possible values for ξ deriving from situations of point contact only: black circles refer to asymmetric point contacts, as in Figure 3, image 4; white squares refer to single point contacts, as in Figure 3, image 1; black triangles refer to symmetric point contacts, as in Figure 3, image 5.

N denotes the number of buckled waves, and $2l_0$ the buckled wavelength. If the relationship between applied axial force and buckled wavelength obeyed a standard Euler theory, the following would hold:

$$l_0 = \frac{\pi}{\alpha}. \tag{3}$$

Euler’s theory is not applicable to this case, however, because of the presence of contact forces between buckled core and external containment profiles.

Introducing a dimensionless parameter ξ to define l_0 in a way similar to (3) as

$$l_0 = \xi \frac{\pi}{\alpha}, \tag{4}$$

the theory developed in [Genna and Bregoli 2014] leads to the results summarized hereafter, valid in the linear elastic case and for frictionless contact.

For the limiting case of $k \rightarrow \infty$, i.e., infinitely rigid retention profiles, $1.4303 \leq \xi \leq 4$ was the range of values that could be obtained for ξ of (4), depending on the buckled configuration assumed by the core.

For finite values of k , the dependency shown in Figure 4 can be computed numerically for the three possible cases of a point contact. In Figure 4, curve (a) refers to the case of an asymmetric point contact,

as in [Figure 3](#), image 2; curve (b) refers to a pure point contact, as in [Figure 3](#), image 1; and curve (c) refers to the case of a symmetric double point contact at each side of the beam, as in [Figure 3](#), image 3. It can be seen that, if only a point contact situation develops, the value of ξ can become very high for small enough values of the stiffness k .

In the presence of a line contact, for any value of the stiffness k , it is proved that $\xi = 3$ in the case of an asymmetric line contact, and $\xi = 4$ in the case of a symmetric line contact.

The actual value of ξ , given a value of the axial shortening, is strongly dependent on the shape of the buckled configuration which, in turn, depends on several factors, among which the imperfections existing in a real structure. Therefore, the actual buckled configuration is theoretically unpredictable, since there are several possible alternatives among which to choose.

Given a buckled configuration, the corresponding expression for the lateral thrust Q can be also computed; the following general result was derived in [[Genna and Bregoli 2014](#)], which gives the unit thrust Q_i , i.e., the contact force existing at each side of a single buckled wave:

$$Q_i = \frac{4\pi\xi\alpha kFs \cos(\pi\xi\beta)}{\cos(\pi\xi\beta)(2\pi^2\xi^2\beta k - \alpha^2 FL) - 2\pi\xi k \sin(\pi\xi\beta)}, \quad (5)$$

where β is a parameter that identifies the length of the inclined portions of the wave between two successive contact points, as shown in [Figure 3](#).

Both in the limiting case $k \rightarrow \infty$, and for all the buckled configurations with incipient or fully formed line contacts, with $\beta = 1/\xi$ as shown in [[Genna and Bregoli 2014](#)], (5) reduces to the trivial one

$$Q_{i,\infty} = \frac{2F\alpha s}{\pi}. \quad (6)$$

In all these expressions, in the presence of a linear elastic material for the core, the value of F is given by (1), and the value of α of (2) is

$$\alpha = \frac{1}{\rho} \sqrt{\frac{\Delta u}{L}}, \quad (7)$$

where ρ is the radius of inertia corresponding to I , i.e., $\rho^2 = I/A$.

The total lateral thrust Q is obtained by multiplying Q_i for the number N of waves in the buckled shape, i.e.,

$$Q = Q_i N, \quad (8)$$

with N an integer number. Genna and Bregoli [[2014](#)] propose to adopt the following expressions for ξ and N , assuming that the containment profiles are stiff enough to allow the formation of line contacts:

$$l_0 = \frac{3\pi}{\alpha}, \quad N = \text{Int}\left(\frac{L}{2l_0} + 0.5\right), \quad (9)$$

where Int denotes the integer part. This result, and specifically the choice $\xi = 3$, defines an axial force nine times larger than the normally adopted Euler one corresponding to a given wavelength $2l_0$ in the linear elastic range.

The analysis in [[Genna and Bregoli 2014](#)] concludes with the observation that an acceptable *engineering* choice for the value of parameter ξ , even in the elastic-plastic range, remains $\xi = 3$, as indicated in (9). In the next two sections, therefore, we will adopt as the best compromise for the value of ξ the value

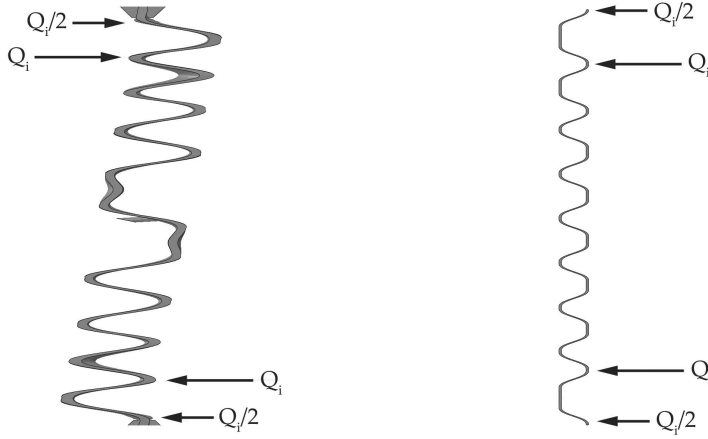


Figure 5. Buckled shapes in two different situations. Left image (from a 3D analysis with ABAQUS): the external containment can undergo rigid rotations. The number of contact points is the same at each side, and the total number of waves is not an integer (8.5, in this image). Right image (from a 2D analysis with ABAQUS in which the containment is described as in Figure 2): the external containment can not rotate. The number of contact points at one side (right, in the figure) is higher by one than at the opposite side; the number of waves is integer (9, in this image).

$\xi = 3$, corresponding to a configuration of asymmetric line contact, and therefore to expression (9) for the wavelength, and to expression (5) for the unit thrust, with $\beta = 1/\xi$. This implies that the containment profiles are stiff enough to enable the development of line contacts. Only Section 5 will discuss possible results deriving from different situations.

In the following, the calculation of the number N of waves associated to l_0 is modified with respect to the result given by (9) proposed in [Genna and Bregoli 2014]. In fact, the examination of both experimental and numerical results (see [Bregoli et al. 2014; Bregoli 2014; Genna and Gelfi 2012a]) shows that it is possible to observe a fractional number of waves, associated to a configuration in which both sides of the core have the same number of contact points. In this case, the number of unit contact forces Q_i , at each side of the core, is of the type $I + 0.5$, with I an integer number, as shown in Figure 5, left image.

This situation derives from a rigid rotation of the external containment case, often possible in real applications but ruled out in the analytical model of [Genna and Bregoli 2014]. This latter must always show an integer number of waves, as in Figure 5, right image, whereas, if a rigid rotation occurs, the configuration can become that of Figure 5, left picture, and the number of waves can be fractional, with a possible difference of \pm half wave with respect to the integer N case. In order to account for this possibility, the suggested expression for N , once computed l_0 , is then

$$N = \frac{1}{2} \text{Int}\left(\frac{L}{l_0} + 0.5\right), \quad (10)$$

which yields a value for N rounded to the closest 0.5.

3. Extension to linear kinematic hardening and cyclic loading

3.1. Linear hardening, monotonic loading. The material parameters describing the plastic properties are now a yield stress of the virgin material, σ_0 , and either a tangent modulus E_t , i.e., the slope of the hardening branch in a uniaxial stress-strain curve, or, equivalently, a hardening coefficient h , i.e., the slope of the hardening branch in a uniaxial stress-plastic strain curve. These parameters are related to each other by the following relationships:

$$E_t = \frac{hE}{E+h}, \quad h = \frac{EE_t}{E-E_t}. \quad (11)$$

In practical BRB applications, the core can undergo only small deflections, since the gap s is assumed to be small. It is then appropriate to consider that, in the plastic range, buckling occurs under increasing axial loading, i.e., with no local unloading at any point of any cross-section of the beam. In this case, Shanley's theory [Shanley 1947] of plastic buckling applies, which, for an Eulerian problem, would imply to replace, in the expression of the buckling load, the Young modulus E with the tangent modulus E_t .

The problem under study is not Eulerian, but Shanley's theory holds also in this case, since the phenomena involved can be seen as a sequence of local Eulerian bucklings in the plastic range. Therefore, in the presence of an elastic-plastic linear hardening material (9) must be modified to

$$l_0 = 3\pi\sqrt{\frac{E_t I}{F}}, \quad (12)$$

where the correct expression for F , assigned a value Δu of the axial shortening, should be adopted, according to the material behavior. Under the assumption of monotonic loading from zero up to an axial shortening Δu , this is done by writing

$$F = A\sigma \quad (13)$$

and

$$\sigma = E_t \left(\bar{\varepsilon} + \frac{\sigma_0}{h} \right), \quad (14)$$

where

$$\bar{\varepsilon} = \frac{\Delta u}{L}. \quad (15)$$

Finally, substituting (13) and (14) into (12), one obtains the desired result:

$$l_0 = \frac{3\pi\rho}{\sqrt{\bar{\varepsilon} + \frac{\sigma_0}{h}}} \quad (16)$$

Result (16) reduces to (9) in the case of linear elasticity ($h \rightarrow \infty$), and yields $l_0 = 0$, i.e., an infinite number of buckled waves, for the case of perfect plasticity ($h = 0$), when, under a compressive axial load at the limit of the carrying capacity of the core, the stiffness vanishes.

In order to obtain the corresponding result for the lateral thrust, one must abandon expression (5), which derives from the linear elastic analysis summarized in Section 2. Recalling that the value $\xi = 3$, in expression (9) of l_0 , derives from a situation of line contact, one has the supplementary information that

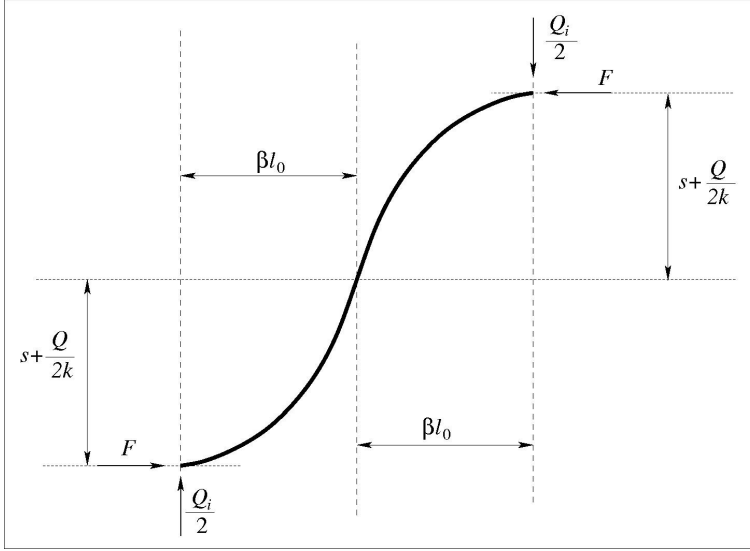


Figure 6. Deformed shape for the calculation of the unit thrust Q_i in all the cases when the bending moment at the contact point vanishes.

the bending moment, at the contact points at both sides of the core, is zero. Therefore, one can compute the unit thrust Q_i directly from equilibrium, as shown in Figure 6, thus obtaining

$$Q_i = \frac{2Fsk}{\beta kl_0 - FN}, \tag{17}$$

which, in the limit $k \rightarrow \infty$, reduces to

$$Q_{i,\infty} = \frac{2Fs}{\beta l_0}. \tag{18}$$

Setting $\xi = 3$ and $\beta = 1/3$ in (17), using (9) for N and (16) for l_0 , one obtains the desired result for the current situation.

3.2. Linear kinematic hardening, cyclic loading. In expression (16) for the buckled wavelength, the driving stress was defined through (14), which holds for monotonic loading only, from zero up to the prescribed axial displacement value.

In the case of cyclic loading, such expression does not hold anymore. One must in fact consider that, after a tension cycle that develops sufficiently large plastic strains, such as is expected to occur in real BRB applications, the core, during the next displacement reversal, and owing to irreversibility, starts being subjected to a compressive axial force while it is still elongated. Buckling is therefore associated to a different starting configuration than in the case of monotonic compressive loading.

This can be accounted for by redefining the current stress, at the end of a compressive loading cycle, as if it were reached following a fictitious monotonic loading condition.

Figure 7 illustrates the problem in terms of a stress-plastic strain diagram. In this plot, where compression and shortening are assumed positive, a loading cycle for a linear kinematic hardening material is considered, as produced by an axial displacement cycle between limits $-\Delta u_t$ and Δu_c (subscripts t

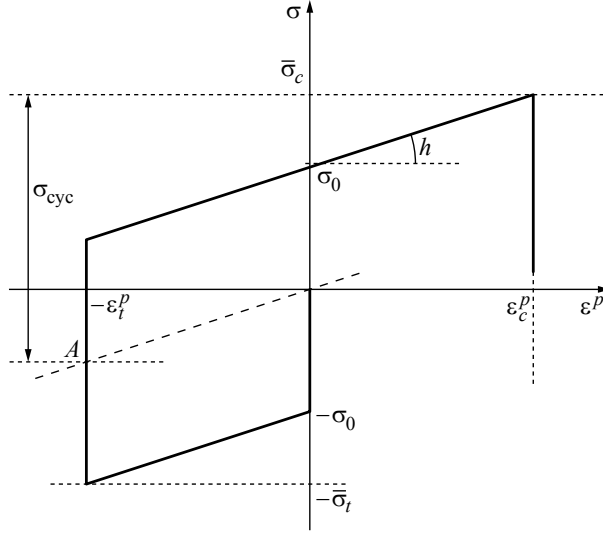


Figure 7. Stress-plastic strain loading cycle with linear kinematic hardening. Definition of σ_{cyc} to be adopted for the calculation of the buckling load in the plastic range under cyclic loading.

and c stand for tension and compression respectively), which correspond to strains $-\bar{\varepsilon}_t$ and $\bar{\varepsilon}_c$, and to plastic strains $-\varepsilon_t^p$ and ε_c^p , respectively. The actual stress values corresponding to the cycle strain limits $\bar{\varepsilon}_c$ and $-\bar{\varepsilon}_t$ would be $\bar{\sigma}_c$ and $-\bar{\sigma}_t$ respectively, both given by an equation of the type of (14).

Expression (16) for l_0 , derived for monotonic loading, can be extended to the case in which the BRB core has undergone the nonmonotonic stress-strain history indicated in Figure 7, that can also include an arbitrary number of previous cycles with the same limits. To do so, a modified stress value must be inserted into equations (13) and (16), replacing the actual stress σ with a fictitious value σ_{cyc} . The stress σ_{cyc} is defined as if the current plastic strain amplitude ε_c^p in compression had been reached monotonically, but starting from point A in Figure 7, after the elastic deformation recovery of the first semicycle in tension.

This leads to the following calculation:

$$\sigma_{cyc} = \sigma_0 + h\varepsilon_c^p + h\varepsilon_t^p = \sigma_0 + h(\bar{\varepsilon}_c - \bar{\varepsilon}_c^e + \bar{\varepsilon}_t - \bar{\varepsilon}_t^e) = \sigma_0 + h\left(\bar{\varepsilon}_c - \frac{\bar{\sigma}_c}{E} + \bar{\varepsilon}_t - \frac{\bar{\sigma}_t}{E}\right). \quad (19)$$

Adopting for $\bar{\sigma}_c$ and $\bar{\sigma}_t$ the expression of (14), one obtains

$$\sigma_{cyc} = E_t \left(\bar{\varepsilon}_c + \bar{\varepsilon}_t + \frac{\sigma_0(E-h)}{Eh} \right). \quad (20)$$

The insertion of result (20) into (16) would allow one to obtain an expression for l_0 holding for any type of cycle. Nevertheless, in the present work we will consider only the special case of cycles of equal amplitude in tension and compression, i.e., $\bar{\varepsilon}_c = \bar{\varepsilon}_t = \bar{\varepsilon}$. This will be done because all the results presented in the next sections will refer to the experimental cycles prescribed by the AISC regulations [AISC 2010], which have equal amplitude in tension and in compression. In such case, it can be immediately seen that

(20) implies a driving strain twice the one holding for monotonic loading:

$$\sigma_{\text{cyc}} = E_t \left(2\bar{\varepsilon} + \frac{\sigma_0(E-h)}{Eh} \right). \quad (21)$$

Restarting from (12) and (13), and replacing expression (21) for the stress into (13), one obtains what follows for the semiwavelength:

$$l_0 = 3\pi\rho \sqrt{\frac{hE}{2\bar{\varepsilon}hE + \sigma_0(E-h)}}. \quad (22)$$

This result must be inserted into (17) for the unit thrust. Nevertheless, since (17) derives just from equilibrium, the expression of the axial force F , in it, should remain the same as in the case of monotonic loading, i.e., (13) with stress σ given by (14).

4. Extension to contact with friction

Coulomb friction is assumed, with friction coefficient μ ; typical values, for BRB applications, are $\mu = 0.15$ for lubricated steel surfaces, and $\mu = 0.25$ for unlubricated steel surfaces, as measured, for instance, in [Genna and Gelfi 2012a].

The correction for including friction amounts to increasing the driving axial compressive force F , associated to the prescribed axial shortening Δu , by the quantity

$$\Delta F = \frac{\mu Q_0}{2}, \quad (23)$$

where Q_0 denotes the total thrust of (8), with Q_i as in (17), computed in the absence of friction, with F associated to the real stress of (14), and l_0 given by (22). This is only a first approximation, which, however, appears to be effective from an engineering viewpoint.

As a consequence, the result for the wavelength should be recomputed replacing, in it, the value of F with $F + \Delta F$. Recalling (12), the final expression for l_0 is thus

$$l_0 = \frac{3\pi\sqrt{E_t I}}{\sqrt{\sigma_{\text{cyc}} A + \mu Q_0/2}}. \quad (24)$$

The same correction to the axial force F must be applied to the formulas for the subsequent calculation of the unit and total thrust, recalling that, in these calculations, the real value of the axial force associated to $\bar{\sigma}$, and increased by friction, should be considered.

We finally summarize the actual procedure to be followed to estimate the total thrust in a real BRB subjected to cyclic loading, variable between equal positive and negative limits (a more general result could be easily obtained adopting (20) for the corrected axial stress at the end of a nonsymmetric loading cycle).

- (1) Compute a first estimate of the wavelength with no friction from (22).
- (2) From this, using (10), compute N_0 , the rounded number of waves associated to the estimated wavelength.

- (3) Recompute a corrected wavelength as

$$l_0^* = \frac{L}{2N_0} \quad (25)$$

associated to the rounded number of waves.

- (4) Recompute corrected values ξ^* and $\beta^* = 1/\xi^*$ from l_0^* , associated to the rounded number of waves. This is done on the basis of definition (4), to be now rewritten in the elastic-plastic, cyclic loading context, i.e., as

$$l_0 = \xi \pi \sqrt{\frac{E_t I}{\sigma_{\text{cyc}} A + \mu Q_0/2}}, \quad (26)$$

with $Q_0 = 0$ for the time being.

- (5) Compute Q_0 from (17) and (8). Recall that, so far, all these quantities hold for the frictionless case; recall also that, in the calculation of the lateral thrust, the expression for the monotonic stress (14) should be adopted when computing the axial force F .
- (6) Compute a first estimate of the actual wavelength, with friction, from (24).
- (7) Compute the correct rounded number of waves, N , using (10).
- (8) Compute the correct wavelength as

$$l_0 = \frac{L}{2N} \quad (27)$$

associated to the rounded number of waves N .

- (9) Compute the correct values for ξ and $\beta = 1/\xi$ from l_0 , associated to the rounded number of waves N , using (26).
- (10) Compute Q_i from (17) and Q from (8), with F associated to the monotonic stress of (14) and increased to consider friction, using the rounded number of waves N .

An analysis of (17), using also (27), shows that the total thrust Q depends on the ratio sb/t , where b is the width and t the height of the core cross-section.

5. Small stiffness of the containment structure

The containment structure, in real BRB applications, has a finite elastic stiffness that derives from the presence of both the connection bolts and the global/local deformability of the profiles employed as a retaining case. Such a stiffness can be taken into account, in the expressions proposed above, by suitably computing the numerical value of the coefficient k , i.e., the elastic stiffness of the connection spring in Figure 2.

Genna and Bregoli [2014] suggest to always use the results holding in the limit $k \rightarrow \infty$, in order to stay clear of the complex behaviors deriving from the use of finite values for k . This implies a corresponding attention in designing a sufficiently stiff containment structure. In fact, if a sufficient stiffness can not be guaranteed, and even ruling out a situation of possible local plastic collapse of the containment profiles, the situation becomes complicated:

- Given a value of Δu , a reduction of k , assuming that the number of buckled waves remains the same, implies an increase of the total thrust, which, in theory, could reach an infinite value.
- Given a value of Δu , a reduction of k might cause a decrease of the number of buckled waves, as shown in Figure 4, and as is intuitive, considering that for $k = 0$ only one wave should appear; if the number of waves is smaller, a smaller thrust is expected.
- Nevertheless, if a change in the number of buckled waves is also associated to a change of the buckled configuration, then it is possible that an opposite effect happens. Consider the curves of Figure 4, for example in the case of a symmetric double point contact configuration: for $k/(\alpha^2 FL) = 0.03$ the predicted value for ξ would be $\xi \approx 3.586287$. If a reduction of the value of k to $k/(\alpha^2 FL) = 0.01$ is considered, then the corresponding value for ξ , for the same configuration, would be $\xi \approx 5.548147$, with a smaller number of waves and a smaller thrust to be expected, according to intuition. But — and here lies the complication — if the value of k becomes small enough, then the occurrence of a double point contact becomes less and less likely, since the confinement structure does not offer enough support for this phenomenon, which can only descend from a previous line contact situation. Therefore, it might well happen that, for $k/(\alpha^2 FL) = 0.01$, a single point contact configuration occurs, for the given value of Δu , to which the value $\xi \approx 3.47089$ corresponds: a number of waves higher even than for the symmetric point contact configuration with $k/(\alpha^2 FL) = 0.03$, and a higher thrust, contrary to the expectations, in the presence of a reduced value for k .

In view of these observations, the following procedure is suggested, for the choice of the appropriate value for ξ in the presence of a given finite value for k : choose the value of ξ from the single point contact curve of Figure 4 (the lowest of the three, with white square symbols), but use always $\xi \geq 3$. This choice seems reasonable because, as said, for small values of k line contacts are less and less expected. According to this criterion, the set of values for ξ shown in Table 1 should be adopted, assuming that even for very small values of k the assumptions underlying the theory hold.

Stiffness k range	ξ
0.00055 < $k/(\alpha^2 FL) \leq 0.000683$	13.49249
0.000683 < $k/(\alpha^2 FL) \leq 0.000725$	12.49189
0.000725 < $k/(\alpha^2 FL) \leq 0.000977$	11.49118
0.000977 < $k/(\alpha^2 FL) \leq 0.00105$	10.49034
0.00105 < $k/(\alpha^2 FL) \leq 0.00151$	9.489326
0.00151 < $k/(\alpha^2 FL) \leq 0.00165$	8.488068
0.00165 < $k/(\alpha^2 FL) \leq 0.00265$	7.486474
0.00265 < $k/(\alpha^2 FL) \leq 0.003$	6.484387
0.003 < $k/(\alpha^2 FL) \leq 0.00583$	5.481536
0.00583 < $k/(\alpha^2 FL) \leq 0.007$	4.477408
0.007 < $k/(\alpha^2 FL) \leq 0.02169$	3.47089
0.02169 < $k/(\alpha^2 FL)$	3

Table 1. Values of the coefficient ξ as a function of the normalized value of the spring stiffness k .

In practice, values $\xi > 5$ should not be expected since, in the case of such small values of the stiffness k , a BRB would hardly behave as it should. In practice, again, all this suggests that the stiffness of the containment structure, given a maximum value of the design axial force, should preferably be not less than the limit value k_{lim} defined by

$$k \geq k_{\text{lim}}, \quad k_{\text{lim}} \approx 0.022\alpha^2 FL, \quad (28)$$

in order to use the “safe” results of the previous section and, at the same time, guarantee for the correct functioning of the BRB.

If use is made of a stiffness-corrected value for ξ from [Table 1](#), if $\xi > 3$ then a point contact configuration is expected, and the value of parameter β , for the calculation of the unit thrust Q_i , must be changed accordingly, since $\beta = 1/\xi$ is valid only for a situation of line contact. The value associated to a single point contact situation is $\beta = 0.5$, as shown in [\[Genna and Bregoli 2014\]](#), and obvious from [Figure 3](#). Apart from the possible redefinition of ξ and β , everything else remains unchanged in the procedure illustrated at the end of the previous section. Even the calculation of Q_i from [\(17\)](#) remains still valid because, in the fully plastic range, the bending moment, at the points of contact, is expected to be always negligible.

[Appendix A](#) illustrates an example of how to compute the stiffness k for a specific arrangement of the containment profiles.

6. Comparison with experimental and numerical results

The proposed analytical procedure has been tested for the reduced-scale BRBs studied in [\[Bregoli et al. 2014; Bregoli 2014; Genna and Gelfi 2012a\]](#). These comprise a steel core plate enclosed into 2 bolted C-shaped steel struts, that act as a retaining case, made of two UPN160 commercial profiles, as shown in [Figure 1](#). Eight different BRB assemblies have been tested: in five of them the steel core has a 50×5 mm cross-section, and in the remaining three the core has a 50×7 mm cross-section. The length of the core is $L = 560$ mm. Five different core-case gap values have been considered: 2×0.25 , 2×0.46 , 2×0.5 , 2×0.70 , and 2×1 mm, i.e., $s = 0.25, 0.46, 0.5, 0.7$, and 1 mm at each side of the core. In the sequel, the different specimens will be denoted, according to the core thickness t and the nominal gap size s , by $5 + 0.25$, $5 + 0.46$, $5 + 0.5$, $5 + 0.7$, $5 + 1$, $7 + 0.25$, $7 + 0.5$, and $7 + 1$. For all the details of these samples, see [\[Bregoli et al. 2014; Bregoli 2014; Genna and Gelfi 2012a\]](#).

The experimental results have been obtained following the AISC prescriptions for the cyclic loading type [\[AISC 2010\]](#). The final step has a value $\Delta u = \pm 11.2$ mm, so as to have, at the end of the last two cycles, $\bar{\varepsilon} = \pm 0.02$ in the core.

Three different arrangements of the retaining profiles have been considered. The basic one, denoted in the following by “design”, makes use of two UPN160 profiles with transversal stiffening ribs welded to them (see [Figure 1](#)). A stiffer geometry has also been tested, denoted by “rigid” in the following, in which an additional longitudinal plate has been welded in the center of the UPN web, along its main axis; the reinforcing plate was doubled, and welded at the thirds of the web length, in the central zone of the assembly. In other cases, also a more deformable assembly was tested, in which no stiffening rib at all was welded to the UPN160 profiles. This setup will be denoted as “Deformable” in the following.

	BRB type	5 + 0.25	5 + 0.46	5 + 0.5	5 + 0.7	5 + 1	7 + 0.25	7 + 0.5	7 + 1
k [N/mm]	“Deformable”	340708	340616	340598	340510	340379	324224	324124	323925
	“Design”	551968	551725	551679	551449	551103	527214	526951	526425
	“Rigid”	671904	671545	671477	671136	670624	643129	642737	641955
F [kN]	“Deformable”	102.6	104.8	105.2	107.3	110.5	141.5	143.2	147.2
	“Design”	102.4	104.4	104.8	106.8	109.7	141.5	143.0	146.8
	“Rigid”	102.3	104.3	104.7	106.6	109.5	141.4	143.0	146.7
	$k \rightarrow \infty$	102.1	103.9	104.3	106.0	108.7	141.3	142.8	146.3
l_0 [mm]	“Deformable”	37.33	37.33	37.33	37.33	37.33	56	56	50.91
	“Design”	37.33	37.33	37.33	37.33	37.33	56	56	50.91
	“Rigid”	37.33	37.33	37.33	37.33	37.33	56	56	50.91
	$k \rightarrow \infty$	37.33	37.33	37.33	37.33	37.33	56	56	50.91
N	“Deformable”	7.5	7.5	7.5	7.5	7.5	5	5	5.5
	“Design”	7.5	7.5	7.5	7.5	7.5	5	5	5.5
	“Rigid”	7.5	7.5	7.5	7.5	7.5	5	5	5.5
	$k \rightarrow \infty$	7.5	7.5	7.5	7.5	7.5	5	5	5.5
Q [kN]	“Deformable”	36.7	70.1	76.8	111.3	167.5	22.5	45.8	107.0
	“Design”	33.8	64.3	70.3	101.4	151.3	21.3	43.4	100.2
	“Rigid”	33.1	62.8	68.6	98.8	147.3	21.0	42.7	98.4
	$k \rightarrow \infty$	30.0	56.7	61.9	88.7	131.3	19.7	40.0	91.0

Table 2. Summary of all the analytical results obtained for the geometries of [Genna and Gelfi 2012a] and [Bregoli 2014].

The reference numerical analyses, which replicate the experimental setup, have been run using the finite element code ABAQUS [Hibbitt et al. 2013], employing a full 3-dimensional mesh for all the parts. The core material was treated as elastic-plastic with nonlinear kinematic hardening; the analysis was run for arbitrarily large displacements and strains, under prescribed displacements. Coulomb friction was defined between the contacting surfaces, with friction coefficient $\mu = 0.15$. More details about the numerical model can be found in [Bregoli 2014].

Simpler numerical analyses have also been run, again using ABAQUS, on planar beam models, in which the containment structure was described by rigid surfaces connected to each other by an elastic spring, and free to translate only. This was done in order to have a direct comparison between the results of the theoretical model and those of finite element simulations adopting exactly the same geometrical and material description. Therefore, in these analyses, that made use of linear Timoshenko beam elements, a linear kinematic hardening model was defined for the core material, and only two loading steps, from 0 to $-\Delta u$ and from $-\Delta u$ to Δu , with $\Delta u = 11.2$ mm, were prescribed. The material parameters describe a metal that corresponds roughly to the real steel of the tests; the yield stress is $\sigma_0 = 330$ MPa and the hardening coefficient is $h = 3850$ MPa. These values have been adopted both for the analytical calculations and for the beam type numerical analyses; the value for the hardening coefficient h was chosen corresponding to the maximum average strain applied to the BRB, i.e., $\bar{\epsilon} = 0.02$, even though the

local strain could reach values twice as larger or more. An initial geometrical imperfection was defined as an irregularity of the axis line of the beam, of the order of $\pm s/600$.

The calculation of the value for the stiffness constant k of the elastic connection spring was done as illustrated in [Appendix A](#), and adopting suitable values for the stiffness of the UPN160 profiles. For the “design” assembly, the value for the moment of inertia of a UPN160 profile, referred to its weakest principal axis, is $I_e = 853000 \text{ mm}^4$. For the case of the “deformable” assembly, in order to estimate the effects of the local deformability of the UPN webs, an equivalent moment of inertia was evaluated numerically, again using ABAQUS for a full 3D model of a single unreinforced UPN160 profile. The result thus obtained is $I_{e,\text{deform}} = 466605 \text{ mm}^4$. Finally, the equivalent moment of inertia of the containment profile, in the “rigid” configuration, was calculated to be $I_{e,\text{rigid}} = 1120000 \text{ mm}^4$.

The value of the bolt stiffness k_B was also taken into account case by case, according to the various bolt geometries and properties.

Inserting all these parameters into (A.4) of [Appendix A](#), one obtains an estimate of the elastic stiffness k of the connection spring in the model of [Figure 2](#). This value was adopted both in the analytical calculations and as a datum for the numerical analyses on the beam models.

[Table 2](#) reports a summary of all the analytical results, as furnished by the procedure illustrated in [Sections 4](#) and [5](#).

The table reports the calculated values of the stiffness k , of the axial force $F + \Delta F$ associated to $\Delta u = 0.02 \text{ mm}$ and accounting for the increase due to friction, of the semiwavelength l_0 , of the wave number N , and of the total lateral thrust Q .

All the effects described in previous work [[Genna and Gelfi 2012a](#); [2012b](#)] can be recognized already for the limiting case of $k \rightarrow \infty$. Moreover, it is seen that, for decreasing values of k , the thrust increases progressively, the wave number remaining always constant.

The maximum difference in the predicted total thrust due to the difference in the external case stiffness occurs in the $5 + 1$ case, and is of about 28% between the “rigid” and the “deformable” setup. This suggests that, for this BRB, the “design” configuration should be appropriate.

[Table 3](#) shows a comparison between the analytical results and the numerical ones given by the planar beam models. The largest differences appear in the cases $s = 1 \text{ mm}$ and for the smaller values of the stiffness k . All the geometries with $s = 1 \text{ mm}$ seem to offer a stronger challenge to the analytical model than the geometries with $s = 0.25 \text{ mm}$. In general, the larger is the gap s the poorer is expected to be the approximation given by the analytical technique. This is due both to increasing lack of validity of a second-order theory and to possible lack of validity of Shanley’s theory. Nevertheless, the analytical results of [Table 3](#) appear always acceptable for sufficiently high values of k .

[Table 4](#) reports a summary of numerical (3D), experimental, and analytical results. In the columns, the superscript (a) indicates that the experimental results have been taken from [[Genna and Gelfi 2012a](#)], whereas the superscript (b) indicates experimental results taken from [[Bregoli 2014](#)]. In both experimental and numerical results, when present, the superscripts (I) and (II) refer to the end of the first and the second compressive cycle of maximum amplitude, respectively. The numerical results refer only to the 3D analyses, that replicate the full AISC cyclic loading history [[AISC 2010](#)]. The analytical results marked as “best k ” are obtained adopting, for the stiffness k , the value corresponding to the actual containment case arrangement, as illustrated previously.

BRB Type	F [kN]		l_0 [mm]		N		Q [kN]	
	Beam model	Anal.	Beam model	Anal.	Beam model	Anal.	Beam model	Anal.
5 + 0.25 “Deformable”	110.5	102.6	35	37.33	8	7.5	67.3	36.7
5 + 0.25 “Design”	106.4	102.4	35	37.33	8	7.5	43.0	33.8
5 + 0.25 “Rigid”	105.9	102.3	35	37.33	8	7.5	38.9	33.0
5 + 0.25 $k \rightarrow \infty$	104.5	102.1	35	37.33	8	7.5	29.0	30.0
5 + 1 “Deformable”	112.1	110.5	40	37.33	7	7.5	101.6	167.5
5 + 1 “Design”	111.8	110.0	40	37.33	7	7.5	99.7	151.3
5 + 1 “Rigid”	111.7	109.5	40	37.33	7	7.5	97.4	147.3
5 + 1 $k \rightarrow \infty$	112.3	108.7	40	37.33	7	7.5	92.5	131.3
7 + 0.25 “Deformable”	146.8	141.5	46.67	56	6	5	38.8	22.5
7 + 0.25 “Design”	145.5	141.5	46.67	56	6	5	29.1	21.3
7 + 0.25 “Rigid”	146.0	141.4	46.67	56	6	5	27.2	21.0
7 + 0.25 $k \rightarrow \infty$	144.5	141.3	46.67	56	6	5	21.9	19.7
7 + 1 “Deformable”	147.9	147.2	46.67	50.91	6	5.5	86.7	107.0
7 + 1 “Design”	150.6	146.8	46.67	50.91	6	5.5	90.4	100.2
7 + 1 “Rigid”	151.1	146.7	46.67	50.91	6	5.5	89.5	98.4
7 + 1 $k \rightarrow \infty$	151.4	146.3	46.67	50.91	6	5.5	82.0	91.0

Table 3. Comparison between analytical predictions and numerical results. These last are given by planar beam models reproducing exactly the assembly of [Figure 2](#), and adopting a linear kinematic hardening material model for the core.

The thrust values Q obtained numerically agree well with the experimental results. In most cases, the analytical results with $k \rightarrow \infty$ provide acceptable estimates of the thrust, whereas the results obtained including a finite value of the stiffness k can be somewhat off the mark, and more so as k decreases and/or the gap s increases, i.e., when the amplitude of the buckled shape increases.

Some analytical results (especially the 5 + 0.25 “deformable” and 7 + 0.25 cases) should be interpreted with caution, because for those there is some uncertainty about the actual value of the nominal gap s , which was not controlled after the BRB assemblage. Nevertheless, considering also that the experimental values of the lateral thrust can change significantly just after a repetition of the same cycle, for the same value of Δu — a phenomenon that has not been described, in the calculations developed here — the overall accuracy of the analytical results appears acceptable from the engineering viewpoint.

As said, there is another effect that influences in a significant way the value of the lateral thrust in BRBs subjected to cyclic loading. As shown also in [Table 4](#), and confirmed by other published and unpublished results, the lateral thrust value depends not only on the current value of the axial shortening Δu , but also on the number of loading cycles applied to the BRB at constant value of Δu . At each repetition of a cycle with the same amplitude, the thrust Q increases, probably as an effect of the accumulation of plastic dissipation, which leads to a progressive change of geometry of the core. One of the consequences of this effect is shown in the last rows of [Table 4](#), which report the increase Δs of the nominal gap, at

		5+0.25			5+0.46	5+0.5		5+0.7	5+1	7+0.25	7+0.5	7+1
		Def. ^(b)	Des. ^(b)	Rigid ^(b)	Des. ^(b)	Des. ^(a)	Rigid ^(b)	Des. ^(b)	Des. ^(a)	Des. ^(a)	Des. ^(a)	Des. ^(a)
F [kN]	Exper.	106.4 ^(I) 108.6 ^(II)	110.5 ^(II)	107.2 ^(I) 108.8 ^(II)	106.5 ^(I) 110.1 ^(II)	121.5	110.1 ^(I) 112.9 ^(II)	106.3 ^(I) 107.4 ^(II)	123.0	158.8	157.4	160.8
	Num.			114.6 ^(I) 114.8 ^(II)	116.4 ^(I) 115.7 ^(II)		121.7 ^(I) 121.7 ^(II)	122.7 ^(I) 106.6 ^(II)				
	Analyt., best k	102.6	102.4	102.3	104.4	104.8	104.7	106.8	109.7	141.5	143.0	146.8
	Analyt., $k \rightarrow \infty$		102.1		103.9	104.3		106.0	108.7	141.3	142.8	146.3
l_0 [mm]	Exper.	37.5 ^(I) 37.33 ^(II)	35 ^(II)	35 ^(II)	33 ^(I) 33 ^(II)	37.3	40 ^(II)	35 ^(I) 35 ^(II)	46.65	50.91	50.91	50.91
	Num.			40 ^(I) 40 ^(II)	40 ^(I) 40 ^(II)		40 ^(I) 40 ^(II)	40 ^(I) 40 ^(II)				
	Analyt., best k	37.33	37.33	37.33	37.33	37.33	37.33	37.33	37.33	56	56	50.91
	Analyt., $k \rightarrow \infty$		37.33		37.33	37.33		37.33	37.33	56	56	50.91
N	Exper.	7.5 ^(II)	8 ^(II)	8 ^(II)	8.5 ^(I) 8.5 ^(II)	7.5	7 ^(II)	8 ^(I) 8 ^(II)	6	5.5	5.5	5.5
	Num.			7.5 ^(I) 7.5 ^(II)	7.5 ^(I) 7.5 ^(II)		7.5 ^(I) 7.5 ^(II)	7.5 ^(I) 7.5 ^(II)				
	Analyt., best k	7.5	7.5	7.5	7.5	7.5	7.5	7.5	7.5	5	5	5.5
	Analyt., $k \rightarrow \infty$		7.5		7.5		7.5	7.5	7.5	5	5	5.5
Q [kN]	Exper.	52.1 ^(I) 61.9 ^(II)	31.4 ^(I) 37.5 ^(II)	35.5 ^(I) 41.3 ^(II)	49.8 ^(I) 66.2 ^(II)	93.7	67.7 ^(I) 77.1 ^(II)	83.3 ^(I) 86.6 ^(II)	136.4	63.6	61.0	121.1
	Num.			32.4 ^(I) 34.2 ^(II)	58.1 ^(I) 61.7 ^(II)		64.7 ^(I) 71.1 ^(II)	89.6 ^(I) 96.7 ^(II)				
	Analyt., best k	36.7	33.8	33.1	64.3	70.3	68.6	101.4	151.3	21.3	43.4	100.2
	Analyt., $k \rightarrow \infty$		30.0		56.7	61.9		88.7	131.3	19.7	40.0	91.0
Δs [mm]	Exper.	1.0	0.09	0.07	0.16		0.18	0.23				
	Num.			0.063	0.14		0.15	0.21				
	Analyt., best k	0.054 (0.216 s)	0.031 (0.124 s)	0.025 (0.1 s)	0.058 (0.126 s)	0.064 (0.128 s)	0.051 (0.102 s)	0.092 (0.131 s)	0.137 (0.137 s)	0.02 (0.086 s)	0.041 (0.082 s)	0.095 (0.095 s)

Table 4. Comparison of numerical, experimental, and analytical results. Numerical results are given by 3D FE models that replicate the experimental setup. Experimental results marked ^(a) are from [Genna and Gelfi 2012a]; those marked ^(b) are from [Bregoli 2014]. Superscript ^I and ^{II} refer to the first and second cycles of maximum amplitude. The rows show, from top to bottom: maximum axial compressive force F ; semiwavelength l_0 ; number N of buckled waves; total lateral thrust Q ; increase Δs in the nominal gap s due to deflection of the containment profiles.

each side of the buckled core, due to the deformation of the external profiles. Both the experimental and numerical results are systematically much higher than the analytical ones. This is certainly due to some inaccuracy in the estimate of the elastic stiffness of the containment structure, as well as to the approximations inherent into the analytical procedure; but it is certainly also due to the fact that the analytical procedure neglects the increase of the lateral thrust produced by the accumulation of plastic strains at each repetition of the same loading cycle. This aspect deserves more attention, and is currently under investigation.

It is worth remarking that even though the analytical predictions for Δs are systematically too small, they indicate a displacement Δs of the order of 10 to 20% of the nominal gap, showing that the deformability of the external profiles plays an important role, that can not be neglected when computing the lateral thrust.

Appendix B will report an example of application of the proposed procedure to a full-scale BRB, in order to illustrate the calculations to be done by an engineer when designing a “real” BRB.

7. Conclusions

The theoretical results developed in [Genna and Bregoli 2014] have been adopted, and suitably extended, to obtain engineering usable estimates for the lateral thrust in steel BRBs. The new expressions derived here for such thrust overcome several important limitations of previous work:

- The elastic stiffness of the containment structure is explicitly accounted for.
- The presence of line contacts is explicitly considered in the expressions for the buckled wavelength.
- An important modification, in the calculation of the buckled wavelength and of the associated value of the lateral thrust, is introduced here, in order to take into account the expected presence of tensile-compressive loading cycles, accompanied by the development of plastic strains of both signs.

All these developments allow for analytical estimates that appear consistently acceptable from the engineering viewpoint, with the important limitation of being valid only in situations implying small buckled amplitudes. Therefore, both cases of a too large nominal gap and/or of an insufficiently stiff containment assembly might prevent the applicability of the analytical technique. A condition was defined to individuate a lower limit of the containment stiffness to be employed, which should be coupled with other possible conditions, such as, for example, the one that guarantees the absence of global buckling or of plastic collapse of the BRB under the prescribed axial shortening.

The analysis of the mechanical behavior of BRBs is a relatively new and challenging research topic, with many aspects to be considered. The present work constitutes an attempt at development and synthesis of previous theoretical work, and should provide a good engineering approach to the analytical calculation of the lateral thrust in steel BRBs. More work is still in progress, concerned with several other topics of interest:

- the accumulation of experimental evidence about several details still not fully explored, such as the dependency of the lateral thrust on the loading history and on several other factors;
- the understanding of the real loading condition to be applied in the analysis of BRBs;
- the development of reasonably accurate yet not too expensive numerical models for this type of problems;

- the acquisition of a deeper understanding of all the theoretical aspects involved in this type of problems; an example of these is suggested, for instance, in [Chai 1998], where it is pointed out that even in the case of a fully conservative situation (linear elasticity for all the materials and frictionless unilateral contact) the postbuckled behavior of BRBs, under loading-unloading cycles, might entail some form of hysteresis loop, of unclear explanation;
- the understanding, both experimentally and numerically, of the low-cycle fatigue behavior of the buckled core, and specially the possibility of predicting the number of cycles before its failure.

All these aspects, for which there is no space in the present work, deserve more study, which is currently under way.

Appendix A: Example of calculation of the spring stiffness k

An example of how to compute a stiffness value k accounting for the elastic stiffness of the containment structure exploits the scheme of Figure 8, which considers two retention profiles with two bolted connections. Other configurations, possibly with more bolts along the containment profiles axis, could be found in practical applications; in these cases it is necessary to suitably modify the expressions proposed next, and, in particular, result (A.1).

One possible way to relate the stiffness k to the stiffness k_B of the connection bolts at each side, and to the elastic bending stiffness $E_e I_e$ of the external profiles, is to make the total displacement η_m , at each side of the model of Figure 2, due to the total thrust Q , equal to the total displacement η_e , at each side of the

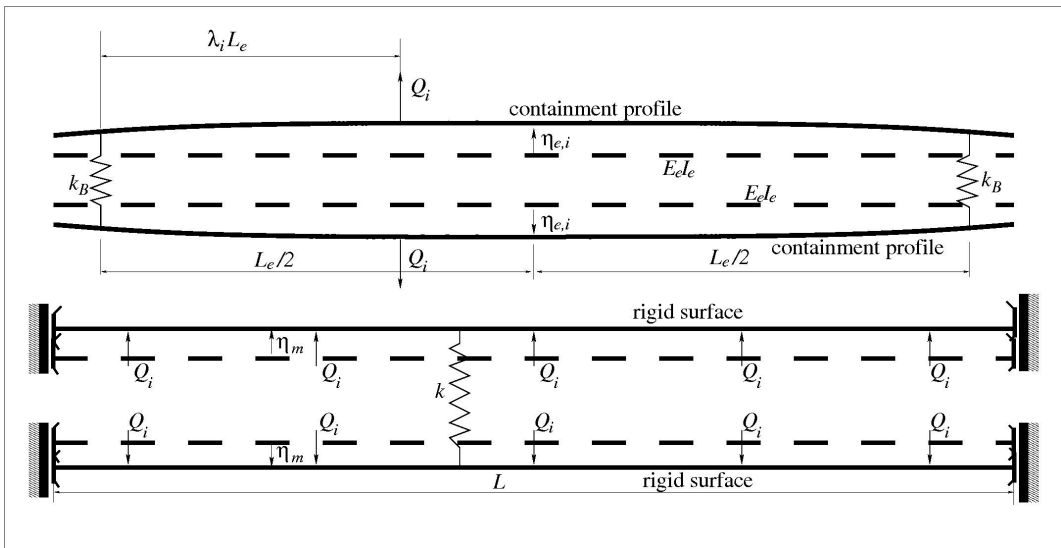


Figure 8. Top image: structural scheme of the external containment structure in the case of two profiles connected by two bolts in the central portion, loaded by a unit thrust Q_i located at an arbitrary position along the BRB length. Bottom image: model of Figure 2, rigid surfaces only, loaded by the total thrust Q . Each rigid surface translates by $\eta_m = Q/(2k)$.

real structural arrangement, under the same thrust, evaluated at the mid-point along the external profile axis. The symbol L_e denotes the distance between the connection bolts in the real structural arrangement. Contact can occur both in the external and in the central portions of the containment profiles, i.e., both outside and between the two bolts.

One can then exploit the assumption of periodicity of the buckled shape of the core, which implies that all the unit thrust forces Q_i have the same value at all the contact points. The displacement $\eta_{e,i}$ at the mid-point of each lateral containment profile, due to a single force Q_i placed at a distance $\lambda_i L$ from its left extremity, with $1 \leq i \leq N/2$, as in [Figure 8](#), has the following expression:

$$\begin{aligned} \eta_{e,i} &= Q_i \left(\frac{1}{4k_B} + \frac{c_{i,e}}{32E_e I_e} + \frac{c_{i,i}}{96E_e I_e} \right), \\ c_{i,e} &= 2\lambda_i L L_e^2 + L_e^3 - L_e^2 L, \quad 0 \leq \lambda_i \leq \frac{L - L_e}{2L}, \\ c_{i,i} &= 2L_e^3 - 3L_e L^2 + L^3 + 12\lambda_i^2 L^2 (L - L_e) - 6\lambda_i L^2 (L - 2L_e) - 8\lambda_i^3 L^3, \\ &\quad \frac{L - L_e}{2L} \leq \lambda_i \leq \frac{1}{2}. \end{aligned} \tag{A.1}$$

Then, the total displacement η_e , due to a number N of unit forces Q_i of equal intensity, has the following expression:

$$\eta_e = Q \left(\frac{1}{4k_B} + \frac{1}{48E_e I_e N} \sum_{i=1}^{N^*} c_{i,e} + \frac{1}{96E_e I_e N} \sum_{i=N^*+1}^N c_{i,i} \right), \tag{A.2}$$

where N^* denotes the number of contact points outside the bolts. Since the corresponding opening in the model of [Figure 2](#) is given by

$$\eta_m = \frac{Q}{2k} \tag{A.3}$$

by equating the results of [\(A.2\)](#) and [\(A.3\)](#) it is immediate to obtain

$$k = \frac{48E_e I_e N k_B}{24E_e I_e N + 3k_B \sum_{i=1}^{N^*} c_{i,e} + k_B \sum_{i=N^*+1}^N c_{i,i}}. \tag{A.4}$$

The values λ_i that appear in coefficients $c_{i,e}$ and $c_{i,i}$ in expressions [\(A.1\)](#) to [\(A.4\)](#) can be easily related to the total number of buckled waves, N , exploiting once more the assumption of periodicity of the buckled shape. One thus finds

$$\lambda_i = \frac{1}{2N} + \frac{i-1}{N}, \quad 0 \leq \lambda_i \leq \frac{1}{2}, \quad 1 \leq i \leq \frac{N}{2}. \tag{A.5}$$

The values of λ_i corresponding to the contact forces located in the right portion of the structure are then obtained from symmetry.

The value for k_B depends on the bolt configuration employed in the real BRB, and is of course related to the elementary expression holding for a single bolt of area A_B , Young modulus E_B and length l_B , i.e.,

$$k_B = \frac{E_B A_B}{l_B}. \tag{A.6}$$

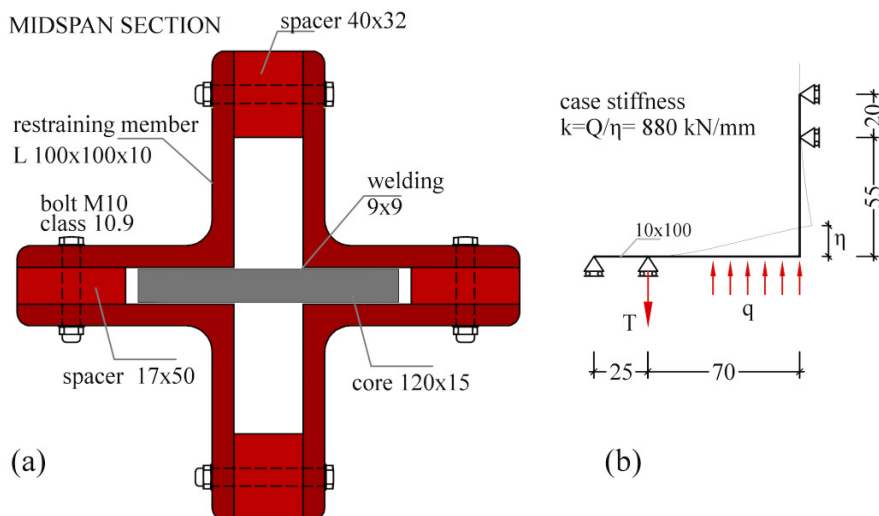


Figure 9. Geometrical details of the section of a full-scale BRB (a); and scheme for the calculation of the case local stiffness (b).

Since the number N of buckled waves is unknown, at the moment of estimating the stiffness k as in (A.4), one must iterate, at least in principle, in order to reach a working expression. One can start from an estimate with $N = 1$, or, better, compute N assuming $k \rightarrow \infty$, and then iterate if necessary to reach a final value for N and then of the total thrust Q .

This elementary calculation has neglected a possible contribution to the elastic stiffness k deriving from the local deformability of the containment at each contact point. This could be due to three-dimensional effects (i.e., plate behavior) possibly important, depending on the actual design of the containment profiles; if necessary, this contribution should be computed case by case adopting specific techniques, either analytical or numerical, for instance based on plate bending theory.

Appendix B: Design of the connecting bolts in a full scale all-steel BRB

This appendix illustrates the design of the bolts connecting the restraining profiles of a real all-steel BRB, following the procedure presented in the paper for the calculation of the lateral thrust exerted by the core during its high-mode buckling. Two cases are presented: in the former, symmetric axial displacement cycles of the BRB core are considered, as occurring in a quasistatic cyclic test following the AISC loading protocol; in the latter, the lateral thrust is calculated for a BRB core undergoing nonsymmetric axial displacement cycles, such as it may happen in reality under a seismic event [Lin et al. 2012].

Figure 9 shows the details of the considered BRB, which was designed and tested at University of Brescia [Gelfi and Metelli 2007]. The brace is 6.0 m long, with a dissipative core length $L = 3.0$ m. The considered gap is $s = 1.0$ mm. The four L-shaped members that act as a retaining structure are connected by means of high strength 10.9 bolts having a diameter of 10 mm, whose spacing must be calculated on the basis of the lateral thrust generated by the core on the restraining profiles. The core is made of

S275 grade steel, with a nominal yield strength $f_{ym} = 321$ MPa. The friction coefficient between the lubricated surfaces is taken equal to $\mu = 0.15$.

This brace is designed to be employed in the first floor of a seven-story building located in a typical medium-seismic zone in Northern Italy (soil type *C*, peak ground acceleration $a_g = 0.20$ g). Details of the design of this BRB are to be found in [Gelfi et al. 2007; Gelfi and Metelli 2007]. The adopted Young modulus of the material is $E = 210000$ MPa; for $\bar{\epsilon} = 0.02$ [AISC 2010], the hardening coefficient was taken equal to $h = 3850$ MPa, and the core yield strength is $f_y = R_y f_{yk} = 1.15 \times 275 = 316$ MPa, $R_y = 1.15$ being the material overstrength factor [AISC 2010]. The restraining member will first be considered as infinitely rigid ($k \rightarrow \infty$), then as having a finite stiffness, in order to highlight the differences entailed by this factor. The calculation of a finite value for the stiffness k is based on the scheme of Figure 9, and was done numerically. The resulting value is $k = 880$ kN/mm.

Example 1: symmetric cycles [AISC 2010]. By considering the BRB core undergoing an average axial core strain $\bar{\epsilon} = 0.02$ with cycles of equal amplitude in tension and compression, as required by the AISC loading protocol, the presented design procedure gives the following results.

- Infinitely rigid containment profiles ($k \rightarrow \infty$):
 - (1) $F = 729$ kN is the maximum axial compressive force accounting also for the increase due to friction;
 - (2) $l_0 = 115.4$ mm is the predicted semiwavelength of the buckled shape under the maximum axial shortening;
 - (3) $N = 13$ is the predicted number of contact points at each side of the core;
 - (4) $q = 0.165$ kN/mm is the predicted lateral thrust per unit length.
- Deformable containment profiles ($k = 880$ kN/mm):
 - (1) $F = 741.5$ kN is the maximum axial compressive force accounting also for the increase due to friction;
 - (2) $l_0 = 115.4$ mm is the predicted semiwavelength of the buckled shape under the maximum axial shortening;
 - (3) $N = 13$ is the predicted number of contact points at each side of the core;
 - (4) $q = 0.237$ kN/mm is the predicted lateral thrust per unit length;
 - (5) $\Delta s = 0.4$ mm is the increase of the gap due to the opening between the containment profiles. Such an increase is the main responsible for the significant increase (order of 40%) of the lateral thrust with respect to the value given by $k \rightarrow \infty$; this shows how, in this case, the deformability of the retaining case plays an important role.

The total tensile force T acting in the bolts is also calculated on the basis of the scheme of Figure 9, including contributions due to the prying action, according to [CEN 2005]. This calculation yields $T = 29.63$ kN. By using high strength bolts ($f_{ub} = 1000$ MPa), two M10 bolts with a longitudinal spacing $p = 100$ mm are needed, having calculated their tensile strength as $F_{t,Rd} = 0.9 f_{ub} A_s / \gamma_{M2} = 41.76$ kN.

It is interesting to compare these results with the corresponding ones obtained experimentally for this type of BRB, that will be described elsewhere. These are: maximum axial compressive force $F = 825$ kN; average value of the buckled semiwavelength $l_0 = 113$ mm; estimated value of the total lateral thrust (not measured experimentally), from (23): $Q = 2\Delta F / \mu = 1080$ kN, where ΔF is the experimentally

measured difference between the peak axial forces in compression and in tension, to be compared with the analytical prediction $Q = qL = 711$ kN for the case of $k = 880$ kN/mm.

Example 2: nonsymmetric displacement cycles. In order to understand the influence of the cycle type on the predicted response of a BRB, we consider now the case of a nonsymmetric axial displacement cycle, such as it is expected to occur under a real seismic event. Lin et al. [2012] report results of tests performed on BRBs subjected to a seismic excitation; from these results it can be seen that, ignoring a possible global shift of the displacement maximum values, the ratio between the maximum tensile average strain and the maximum compressive one, in a typical cycle, is of about 0.375. Therefore, we keep fixed the value $\bar{\epsilon} = 0.02$ as the maximum compressive axial strain, which governs the current value of the axial force, but we consider a strain cycle ranging between $-\bar{\epsilon}_t = -0.007$ and $\bar{\epsilon}_c = 0.02$. Therefore, use is made of (20) instead of (21) to calculate the driving stress for the calculation of the wavelength. The corresponding results are as follows.

- Infinitely rigid containment profiles ($k \rightarrow \infty$):
 - (1) $F = 727$ kN is the maximum axial compressive force accounting also for the increase due to friction;
 - (2) $l_0 = 120$ mm is the predicted semiwavelength of the buckled shape under the maximum axial shortening;
 - (3) $N = 12.5$ is the predicted number of contact points at each side of the core;
 - (4) $q = 0.149$ kN/mm is the predicted lateral thrust per unit length.
- Deformable containment profiles ($k = 880$ kN/mm):
 - (1) $F = 735$ kN is the maximum axial compressive force accounting also for the increase due to friction;
 - (2) $l_0 = 120$ mm is the predicted semiwavelength of the buckled shape under the maximum axial shortening;
 - (3) $N = 12.5$ is the predicted number of contact points at each side of the core;
 - (4) $q = 0.205$ kN/mm is the predicted lateral thrust per unit length;
 - (5) $\Delta s = 0.35$ mm is the increase of the gap due to the opening between the containment profiles.

The compressive axial force remains, as expected, practically unaltered, with respect to the case of symmetric cycles ending to the same shortening displacement; the lateral thrust reduces of about 15%, as a consequence of the reduced strain excursion in tension. Since the design of this element must comply with the AISC regulations, which prescribe tests under symmetrical loading cycles, this last set of calculations should be seen only as a check, and not as a design procedure.

Acknowledgments

This work was done with the support of the Italian Ministry of Education and Research (MIUR). The authors express their thanks to Dr. Marco Baiguera for his help with both the experimental and the numerical part of the work.

References

[AISC 2010] *Seismic provisions for structural steel buildings*, American Institute of Steel Construction, Chicago, USA, 2010.

- [Bregoli 2014] G. Bregoli, *Studio di dispositivi in acciaio per il miglioramento sismico di edifici in C.A.*, Ph.D. thesis, University of Brescia, Italy, 2014.
- [Bregoli et al. 2014] G. Bregoli, M. Baiguera, G. Metelli, and F. Genna, “Experimental and numerical analysis on the core lateral thrust in bolted BRBs”, in *Proceedings of the 7th European Conference on Steel and Composite Structures (EUROSTEEL 2014)* (Napoli, Italy, 2014), University of Naples Federico II, 2014.
- [CEN 2005] “EN1993-1-8 — Eurocode 3: design of steel structures, 1–8: design of joints”, technical report, European Committee for Standardization, Brussels, 2005, Available at <http://www.eurocodes.fi/1993-1-8/SFS-EN1993-1-8-AC.pdf>.
- [Chai 1998] H. Chai, “The post-buckling response of a bi-laterally constrained column”, *J. Mech. Phys. Solids* **46**:7 (1998), 1155 – 1181.
- [Chou and Chen 2010] C.-C. Chou and S.-Y. Chen, “Subassemblage tests and finite element analyses of sandwiched buckling-restrained braces”, *Eng. Struct.* **32**:8 (2010), 2108 – 2121.
- [Gelfi and Metelli 2007] P. Gelfi and G. Metelli, “Prova sperimentale di un elemento diagonale di controvento ad instabilità controllata”, pp. 169–176 in *Atti del XXI Congresso C.T.A.: Costruire con l’Acciaio* (Catania, Italy, 2007), edited by A. Ghersi, Logo Flaccovio, Milan, 2007.
- [Gelfi et al. 2007] P. Gelfi, E. Marchina, G. Metelli, and A. Temponi, “Studio teorico e sperimentale sui controventi concentrici ad instabilità impedita”, technical report, no. 5, DICATAM, University of Brescia, Brescia, Italy, 2007.
- [Genna and Bregoli 2014] F. Genna and G. Bregoli, “Small amplitude elastic buckling of a beam under monotonic axial loading, with frictionless contact against movable rigid surfaces”, *JOMMS* **9**:4 (2014), 441–463.
- [Genna and Gelfi 2012a] F. Genna and P. Gelfi, “Analysis of the lateral thrust in bolted steel buckling-restrained braces, I: experimental and numerical results”, *J. Struct. Eng. (ASCE)* **138**:10 (2012), 1231–1243.
- [Genna and Gelfi 2012b] F. Genna and P. Gelfi, “Analysis of the lateral thrust in bolted steel buckling-restrained braces, II: engineering analytical estimates”, *J. Struct. Eng. (ASCE)* **138**:10 (2012), 1244–1254.
- [Hibbitt et al. 2013] H. Hibbitt, B. Karlsson, and P. Sorensen, “ABAQUS User’s Manual”, Software manual (release 6.12), Dassault Systèmes, Simulia Corp, Providence, RI, 2013.
- [Lin et al. 2012] P.-C. Lin, K.-C. Tsai, K.-J. Wang, Y.-J. Yu, C.-Y. Wei, A.-C. Wu, C.-Y. Tsai, C.-H. Lin, J.-C. Chen, A. H. Schellenberg, S. A. Mahin, and C. W. Roeder, “Seismic design and hybrid tests of a full-scale three-story buckling-restrained braced frame using welded end connections and thin profile”, *Earthq. Eng. Struct. Dyn.* **41**:5 (2012), 1001–1020.
- [Shanley 1947] F. Shanley, “Inelastic column theory”, *J. Aeronaut. Sci.* **14** (1947), 261–268.
- [Takeuchi et al. 2010] T. Takeuchi, J. Hajjar, R. Matsui, K. Nishimoto, and I. Aiken, “Local buckling restraint condition for core plates in buckling restrained braces”, *J. Constr. Steel Res.* **66**:2 (2010), 139–149.
- [Wu et al. 2014] A.-C. Wu, P.-C. Lin, and K.-C. Tsai, “High-mode buckling responses of buckling-restrained brace core plates”, *Earthq. Eng. Struct. Dyn.* **43**:3 (2014), 375–393.
- [Zhao et al. 2014] J. Zhao, B. Wu, W. Li, and J. Ou, “Local buckling behavior of steel angle core members in buckling-restrained braces: cyclic tests, theoretical analysis, and design recommendations”, *Eng. Struct.* **66** (2014), 129–145.

Received 6 Oct 2015. Revised 17 Nov 2015. Accepted 24 Nov 2015.

GUIDO BREGOLI: g.bregoli@unibs.it

Department of Civil Engineering, University of Brescia, Via Branze, 43, I-25123 Brescia, Italy

FRANCESCO GENNA: francesco.genna@unibs.it

Department of Civil Engineering, University of Brescia, Via Branze 43, I-25123 Brescia, Italy

GIOVANNI METELLI: giovanni.metelli@unibs.it

Department of Civil Engineering, University of Brescia, Via Branze, 43, I-25123 Brescia, Italy

JOURNAL OF MECHANICS OF MATERIALS AND STRUCTURES

msp.org/jomms

Founded by Charles R. Steele and Marie-Louise Steele

EDITORIAL BOARD

ADAIR R. AGUIAR	University of São Paulo at São Carlos, Brazil
KATIA BERTOLDI	Harvard University, USA
DAVIDE BIGONI	University of Trento, Italy
YIBIN FU	Keele University, UK
IWONA JASIUK	University of Illinois at Urbana-Champaign, USA
C. W. LIM	City University of Hong Kong
THOMAS J. PENCE	Michigan State University, USA
DAVID STEIGMANN	University of California at Berkeley, USA

ADVISORY BOARD

J. P. CARTER	University of Sydney, Australia
D. H. HODGES	Georgia Institute of Technology, USA
J. HUTCHINSON	Harvard University, USA
D. PAMPLONA	Universidade Católica do Rio de Janeiro, Brazil
M. B. RUBIN	Technion, Haifa, Israel

PRODUCTION production@msp.org

SILVIO LEVY Scientific Editor


Cover photo: Mando Gomez, www.mandolux.com

See msp.org/jomms for submission guidelines.

JoMMS (ISSN 1559-3959) at Mathematical Sciences Publishers, 798 Evans Hall #6840, c/o University of California, Berkeley, CA 94720-3840, is published in 10 issues a year. The subscription price for 2016 is US\$575/year for the electronic version, and \$735/year (+\$60, if shipping outside the US) for print and electronic. Subscriptions, requests for back issues, and changes of address should be sent to MSP.

JoMMS peer-review and production is managed by EditFLOW[®] from Mathematical Sciences Publishers.

PUBLISHED BY

 **mathematical sciences publishers**
nonprofit scientific publishing

<http://msp.org/>

© 2016 Mathematical Sciences Publishers

Journal of Mechanics of Materials and Structures

Volume 11, No. 2

March 2016

- The effect of small scale on the free vibration of functionally graded truncated conical shells** **YAGHOUB TADI BENI and FAHIMEH MEHRALIAN** **91**
- Conditions for the localisation of plastic deformation in temperature sensitive viscoplastic materials** **MARTIN K. PAESOLD, ANDREW P. BASSOM, KLAUS REGENAUER-LIEB and MANOLIS VEVEAKIS** **113**
- A simple hard-particle collision model with a smooth transition to full slip** **M. B. RUBIN** **137**
- Multiobjective optimization of laminated composite plate with elliptical cut-out using ANN based NSGA-II** **P. EMMANUEL NICHOLAS, M. C. LENIN BABU and A. SATHYA SOFIA** **157**
- Analytical estimates for the lateral thrust in bolted steel buckling-restrained braces** **GUIDO BREGOLI, FRANCESCO GENNA and GIOVANNI METELLI** **173**